62 72250 Copy
NASA TM X-426
UNCLASSIFIED
NASA TM X-426
Declassified by authority of NASA
Classification Change Notices No. 1 & 3
dated ** 2-1-61

TECHNICAL MEMORANDUM

X-426 DECLASSIFIED- 1/31/68
AUTHORITY- TAINE TO SHAUKLAS
MEMO. US: 2840 dated 2/6/68

INVESTIGATION OF THE AERODYNAMIC CHARACTERISTICS OF A REENTRY CAPSULE WITH VARIOUS NOSE SHAPES AT A MACH NUMBER OF 2.91, INCLUDING STUDIES OF NOSE SPIKES AS A MEANS OF CONTROL

By Richard W. Harman and William B. Boatright

Langley Research Center
Langley Field, Va.

FACILITY FORM 602
(ACCESSION NUMBER) (THRU)
(PAGES) (CODE)
(NASA CR OR TMX OR AD NUMBER) (CATEGORY)

NATIONAL AERONAUTICS AND SPACE ADMINISTRATION
WASHINGTON
January 1961

DECLASSIFIED

NATIONAL AERONAUTICS AND SPACE ADMINISTRATION

TECHNICAL MEMORANDUM X-426

INVESTIGATION OF THE AERODYNAMIC CHARACTERISTICS OF A REENTRY CAPSULE WITH VARIOUS NOSE SHAPES AT A MACH NUMBER OF 2.91, INCLUDING STUDIES OF NOSE SPIKES AS A MEANS OF CONTROL*

By Richard W. Harman and William B. Boatright

SUMMARY

The lift, drag, and pitching moment have been measured for a reentry capsule with several series of nose shapes. All models had the same afterbody shape. One series of models was used to determine the effects of nose fineness ratio on the aerodynamic characteristics for nose shapes consisting of spherically blunted cones. Nose shapes with semiapex angles of 90°, 70°, 50°, 30°, 20°, and 16° were tested. A second series of models had asymmetrical nose shapes. For this series the spherically blunted apexes of a 30° and a 50° half-angle cone were each offset 1/3, 2/3, and 1 capsule radius. Tests were conducted on a third series of models with a spherical-segment nose shape canted 0°, 7°, 14°, and 21°. In a fourth series preliminary information was obtained on the use of a spike protruding from the nose of a capsule as a means of producing lift and control forces. All tests were conducted through an angle-of-attack range of about -16° to 16°. For some configurations the experimental results were compared with modified Newtonian theory.

Results of nose fineness-ratio tests showed that lift-drag ratios of about -0.2 were obtained with blunt models and a lift-drag ratio of about 0.8 was obtained with the slender 16° conical-nosed model. A cross plot of the data revealed that if the cone half-angle were about 42°, no lift would be generated as angle of attack varied. Both the model with the largest nose cant and the model with the largest nose offset produced a lift-drag ratio of about 0.5. There was no effect on the linearity or slope of the pitching-moment variation with angle of attack due to canting the nose or offsetting the apex. High-frequency oscillatory flow (about 500 to 600 cps) occurred during the tests with some of the nose-spike models. The forces and moments produced by the spikes were very nonlinear.

*Title, Unclassified.

[redacted]

INTRODUCTION

As contrasted to the nonlifting reentry body following a ballistic trajectory, the use of lift during a reentry maneuver lowers the deceleration forces and improves touchdown accuracy. Since even small values of lift coefficient can produce fairly large changes in these deceleration forces and provide the vehicle with an increased choice of landing site, the lifting body appears worthy of close consideration for certain missions. In addition to its potential value as a vehicle for manned reentry from near-earth orbits (ref. 1), the lifting body has possible applications to those missions in which a ballistic type of reentry is not feasible. For example, the high reentering velocities of a vehicle returning from a lunar mission might require the use of lift to lower the deceleration forces to acceptable levels even for unmanned vehicles. Also, a vehicle returning to earth from a lunar mission would probably not be able to start the reentry maneuver with the accuracy of a near-earth satellite and the use of lift during the atmospheric portion of reentry might be mandatory in order to improve touchdown accuracy. The improvement of touchdown accuracy would ease the guidance and retro-rocket time-of-firing requirements to assure that the vehicle landed where desired.

The purpose of this investigation was to obtain quantitative information on methods of providing lifting capabilities to a reentry capsule in order to determine the nose shape that is most effective and trouble-free in producing lift. The effect of nose fineness ratio, the effect of offsetting the spherically blunted apex of a conical nose, and the effect of canting a nose composed of a spherical segment were investigated. All configurations had the same afterbody shape. Also, a preliminary investigation was made to explore the use of a spike protruding from the different nose shapes as a means of generating lift or control forces. The tests were conducted at a Mach number of 2.91. This Mach number was not too low for assessing the hypersonic aerodynamic characteristics of the different nose shapes since the noses were blunt. In a number of cases the results were compared with Newtonian theory, and the agreement with theory also indicates that the Mach number was not too low.

SYMBOLS

The data are referred to the stability-axis system with the moment reference at a point 0.520 inch behind the maximum diameter unless otherwise noted.

C_D	drag coefficient, Drag/qA
$C_{D,o}$	zero-lift drag coefficient
$C_{D,90^o}$	drag coefficient of flat plate at 90° to free stream
C_L	lift coefficient, Lift/qA
C_m	pitching-moment coefficient, Pitching moment/qAd
$C_{m_\alpha} = dC_m/d\alpha$	
C_N	normal-force coefficient, Normal force/qA
$C_{p,max}$	maximum pressure coefficient on nose of body
d	maximum diameter of model
l	length of spike, in.
L/D	lift-drag ratio
M	Mach number
p	static pressure, lb/sq in.
q	dynamic pressure, lb/sq in.
r	nose radius of model, in.
R	Reynolds number (based on maximum diameter)
A	maximum cross-sectional area, sq in.
V	free-stream velocity
α	angle of attack, deg
δ	spike deflection, deg
θ_c	nose-cone half-angle, deg

Subscripts:

b	base
cp	center of pressure
∞	free stream

APPARATUS AND TESTS

Wind Tunnel, Balance, and Model Support

The investigation was conducted in the Langley 9-inch supersonic tunnel of the High-Temperature Fluid Mechanics Section. This is a continuous, closed-return type of tunnel with provisions for the control of the humidity, temperature, and pressure of the enclosed air. During the tests the quantity of water vapor in the tunnel air was kept sufficiently low so that the effect of water condensation in the supersonic nozzle was negligible.

The balance system used in these tests was of a six-component, external type which utilized mechanical self-balancing beams for force measurements. A detailed description of this balance system is presented in the appendix of reference 2.

The models were sting mounted to the model support of the external balance system. The stings were shielded from air loads by a movable windshield which was equipped with four pressure tubes open at the snout of the windshield, behind the model base, to measure model base pressures. The streamwise gap between the base of the models and the snout of the windshield was maintained at about 0.015 inch or less for all tests.

Models

General.- Four series of models were tested. The first series was selected to evaluate the effect of nose fineness ratio of the aerodynamic characteristics of the capsule. The second series was designed to evaluate the effect of offsetting the spherically blunted apex of the conical nose. The third series used nose cant to produce lift. The fourth series was designed to determine the effects of spikes of varying lengths and deflections protruding from the center of the nose on the aerodynamic and control characteristics of a capsule.

Nose fineness-ratio series.- Drawings of the nose shapes of this series are shown in figure 1(a). This series consisted of six interchangeable nose shapes mounted on a common afterbody. The six nose shapes included a flat plate and five blunted conical nose shapes. The semiapex angles of the conical shapes were 70°, 50°, 30°, 20°, and 16°. All the conical nose shapes were spherically blunted with a 0.25-inch-radius sphere tangent to the conical surface.

Nose apex-offset series.- The 50° and 30° nose half-angle shapes pictured in figure 1(a) were used to study the effect of offsetting the apex of the nose. As shown in figure 1(b), the apex was offset 1/3, 2/3, and 1 capsule radius. Each of these different nose shapes had the same afterbody shape as was used in the nose fineness-ratio series.

Nose-cant series.- The third series consisted of four capsules with nose-cant angles of 0°, 7°, 14°, and 21° (fig. 1(c)). The nose shape used was a spherical segment with a 2.148-inch radius.

Nose-spike series.- Three nose shapes (a flat plate (model 0-A), a 20° blunted conical nose (model 4-A), and a 70° blunted conical nose (model 1-A)) were used in the fourth series in order to evaluate the effects of nose spikes. A 3/32-inch-diameter spike was installed in the center of the apex of each nose as shown in figure 1(d). Spike lengths of 0.75, 1.50, and 2.25 inches were tested. Tests were also conducted with the spikes deflected at angles of 0°, 10°, and 20°.

Test Conditions and Procedures

Tests were made at a Mach number of 2.91 and a Reynolds number of 0.78×10^6. One test was conducted wherein the Reynolds number was varied from 0.26×10^6 to 1.14×10^6. All configurations were tested through an angle-of-attack range of -15° to 17°.

Measurements, Corrections, and Accuracy

Lift, drag, and pitching moment were measured on the external balance system. The angle of attack of the models was determined with an optical system which used a small (1/16-inch-diameter) mirror attached to the models near the rear of the afterbody. These mirrors reflected an image from the external light source onto a graduated scale.

Standard corrections for sting-mounted models in the Langley 9-inch supersonic tunnel were applied to the drag data of the configurations to

account for the difference between free-stream pressure and (1) the measured pressure on the base of the afterbody and (2) the pressure on the fixed-windshield balance-box enclosure. This correction amounted to correcting the model base pressure to free-stream static pressure or to zero base drag.

The probable accuracies of the data, based solely on balance calibration are estimated to be within the following limits:

C_L	±0.001
C_D	±0.0002
C_m	±0.005
L/D	±0.15
M	±0.01
α, deg	±0.05
R	$\pm 0.02 \times 10^6$

RESULTS AND DISCUSSION

Effects of Nose Fineness Ratio

Schlieren photographs.- Schlieren photographs illustrating the shock structure for the noses of different fineness ratio are shown in figure 2. In addition to the expected variations in shock shape and detachment distance it can be seen that the nose shape influences the converging angle of the mixing boundary (that is, the extent of separated flow over the afterbody) which envelopes the afterbody. For the blunter nose shapes (models 0-A and 1-A) this boundary is well away from the afterbody, whereas for the higher fineness ratios (models 4-A and 5-A) the mixing boundary is very close to the afterbody surface.

Basic aerodynamic characteristics.- The basic aerodynamic characteristics of the capsule with each nose shape of the fineness-ratio series are shown in figure 3. The blunter shapes (models 0-A, 1-A, and 2-A) have a negative lift-curve slope, whereas the more slender nose shapes produce a positive lift-curve slope. The negative lift-curve slope, of course, simply results from the fact that at positive angles of attack there is a large axial force on the front face of the blunter noses which has a component in the negative lift direction that is larger than the positive lift component of the normal force. As the nose shape becomes more slender the axial-force contribution of the nose diminishes, and at some specific cone angle the nose produces

the conventional positive lift at positive angles of attack. A cross plot of the data shown in figure 3 indicates that a cone half-angle of about 42° would be needed for a configuration to produce a lift-curve slope of zero. This, of course, would apply only to configurations with the specific afterbody shape used in this investigation.

An approximation to the size and direction of the afterbody lift can be conveniently made for model 0-A by using the pressure-distribution data for a flat-faced cylinder presented in reference 3. Reference 3 shows that the ratio of the local pressure to the normal-shock pressure over a flat face is independent of Mach number between Mach numbers of 2.49 and 4.44. By using the data presented in reference 3, the force on a flat face at $\alpha = 15^\circ$ is determined to be about 0.82 of the force which would exist if the pressure behind a normal shock acted over the entire face. Therefore this force would produce a lift coefficient C_L of about -0.37 for model 0-A at $\alpha = 15^\circ$. The experimentally measured lift coefficient at $\alpha = 15^\circ$ for model 0-A was -0.35. This illustrates that the lift on the afterbody was essentially zero. How well this estimate of afterbody lift can be applied to the other configurations is uncertain.

Figure 3 shows a comparison of the lift-coefficient data of shapes 1-A and 5-A with a theoretical prediction based on modified Newtonian theory. The agreement between experimental results and theory is very good. Since the theory did not account for any afterbody the agreement might be fortuituous to some extent; however, it has been previously shown that the afterbody lift for shape 0-A was essentially zero.

The drag-coefficient data shown in figure 3 for the various nose shapes illustrate the large reductions in drag which can be obtained by increasing the fineness ratio of the nose. Figure 3 also shows the expected result that the models with the negative lift-curve slopes (0-A, 1-A, and 2-A) have an inverse variation of drag with angle of attack, whereas the models with more slender nose shapes have the conventional drag-curve shape. The drag prediction of modified Newtonian theory appears good for shape 1-A but this theory underpredicts the drag for shape 5-A. In each case, however, the variation of drag coefficient with angle of attack is well predicted. The experimental drag coefficients have been corrected to zero base drag coefficient only on the base of the model. However, modified Newtonian theory assumes that free-stream pressure also acts on the conical afterbody. The fact that the conical afterbody produces only a small contribution to the experimental drag coefficient at $\alpha = 0^\circ$ can be seen by the following simple breakdown of the drag acting on the flat-faced model (0-A). For this model, if the pressure-distribution data presented in reference 3

L 9 3 2

[redacted]

are used to determine the drag coefficient due to the front face at $\alpha = 0^\circ$, the resulting drag coefficient C_D is 1.58. The measured $C_{D,o}$ shown in figure 3 is 1.68. The fact that the difference is so small indicates that the conical afterbody makes a very minor contribution to the drag and hence has essentially free-stream pressure acting on it.

Comparison of drag with theory.- The effect of the nose fineness ratio or slenderness on the minimum drag coefficient can be seen in figure 4. By using modified Newtonian theory the drag coefficient of a cone may be expressed as

L 9 3 2

$$C_D = C_{p,max}\sin^2\theta_c$$

or

$$\frac{C_D}{C_{D,90^\circ}} = \sin^2\theta_c$$

The line shown in figure 4 with a slope of 1.0 would thus be the Newtonian approximation of the drag for sharp-nosed cones. Also shown in figure 4 are the experimental drag-coefficient data and the theoretical drag variation of sharp cones based on the cone theory presented in reference 4. The experimental drag coefficients for the capsules with the large nose fineness ratios (models 3-A, 4-A, and 5-A) are greater than the predictions of either the Newtonian approximation or the more exact theory of reference 4.

For these more slender configurations it is generally known that the theory of reference 4 is very good. Also, since the afterbody drag is probably fairly close to zero, the larger drag values shown by the data as compared with the prediction of reference 4 must be for the most part due to blunting the cones. Model 2-A, which has a cone angle almost exactly that which is necessary to produce shock detachment, has less drag than is predicted by the theory of reference 4, but greater drag than the Newtonian prediction for a sharp-nosed cone.

Lift-drag ratio.- The effect of fineness ratio on the lift-drag ratio is shown in figure 3. These curves illustrate that lift-drag ratios of about 0.8 can be obtained for the models with noses of large fineness ratio. Lift-drag ratios of about -0.2 can be obtained with the blunt-faced models. Model 2-A, which had an intermediate nose fineness ratio, produced the least lift-drag ratio of any model tested.

Pitching moment.- The moment-coefficient data shown in figure 3 have been referenced to a point which is a fixed distance (0.52 inch)

[redacted]

behind the maximum diameter of the model. The curves for models 0-A, 1-A, and 2-A have a slightly negative slope. However, as might be expected, the slopes of the curves for models 3-A, 4-A, and 5-A become increasingly positive as fineness ratio is increased. Figure 5(a) shows the variation of C_m with C_L for the models with varying nose fineness ratio. The curves for the blunter models (0-A, 1-A, and 2-A) have almost zero slope; the curves for models 3-A, 4-A, and 5-A have a positive slope which increases as nose fineness ratio increases. Figure 5(b) shows the variation of center of pressure with angle of attack. Model 2-A, which generates the least lift of any model tested, has the most nonlinear center-of-pressure variation.

As might be expected, figure 3 shows that C_m increases with increase in nose fineness ratio; this occurs since lifting area is added ahead of the fixed-moment reference location as nose fineness ratio is increased. However, figure 6(a) shows that if the center of planform area is used as the moment reference for each model, the models with larger fineness ratio are still unstable. A summary of the effect of nose fineness ratio on stability is presented in figure 6(b) by plotting C_{m_α} as a function of nose-cone half-angle for the data with fixed moment reference and the data with the moment reference at the center of planform area. This figure illustrates that with the fixed moment reference (0.52 inch behind the maximum diameter), the configurations would be unstable for cone half-angles less than 50° and stable for larger cone angles. The data with the moment-reference location taken at the center of planform area indicate that configurations with cone half-angles less than about 40° would be unstable and that configurations blunter than this would be stable. It will be remembered that the cone half-angle for zero lift-curve slope occurred at about 42°.

Effects of Nose Apex Offset

One means of generating lift on a reentry capsule is to design it with an asymmetrical nose. A preliminary evaluation was made of the lift and stability characteristics which can be produced in this way. The nose shapes used in the evaluation are shown in figure 1(b). These nose shapes were tested in conjunction with the same afterbody as was used in evaluating nose fineness-ratio effects. Models 2-B, 2-C, and 2-D were modified versions of model 2-A but with the nose apex offset 1/3, 2/3, and 1 maximum radius, respectively. Models 3-B, 3-C, and 3-D were similar modifications of model 3-A.

Figure 7(a) shows the aerodynamic characteristics of models 2-A, 2-B, 2-C, and 2-D, and figure 7(b) shows these characteristics for models 3-A, 3-B, 3-C, and 3-D. The data show that large amounts of

lift can be realized with these models and that the lift increases with increasing nose offset. For the blunter models (fig. 7(a)), the drag increases with increasing nose offset at angles of attack greater than -6°; however, there is still an increment in lift-drag ratio with increasing nose offset. Offsetting the apex of the capsule with a 30° half-angle conical nose by the full capsule radius produced a lift-drag ratio of about 0.5 at an angle of attack of 0°. At angles of attack less than -6° the drag is less for an offset of 1 maximum radius than for an offset of 2/3 maximum radius. Near $\alpha = 0^{\circ}$ the models with the 30° conical nose (figure 7(b)) have larger increases in lift due to nose offset than the blunter models (figure 7(a)), and higher lift-drag ratios are obtained. At angles of attack above -14° the drag increases as nose offset is increased from 1/3 to 1 maximum radius. For all models with the 30° nose the drag coefficient was lowered in the negative angle-of-attack range by using any amount of nose offset, and one model (3-B) had a drag coefficient less than the drag coefficient for an axisymmetric model (3-A) throughout the complete angle-of-attack range for which tests were conducted.

The pitching-moment results presented in figure 7 show that there is no increase in the nonlinearity of the curves due to nose offset. Also, nose offset has essentially no effect on the slope of the pitching-moment curves. A positive increment in the magnitude of the pitching moment is produced by each successive increase in nose offset, however, and this increment is larger for the models with the more slender nose.

Effects of Nose Cant

A sketch of each of the four models which were tested to evaluate the effects of nose cant is shown in figure 1(c). The aerodynamic characteristics of these models are shown in figure 8. The reference area for the aerodynamic coefficients shown in figure 8(a) was the maximum cross-sectional area at the nose-afterbody juncture of the model with 0° cant. At an angle of attack of 0° the increase in lift due to canting the nose varies linearly with increasing cant angle and a lift-coefficient increment of about 0.021 per degree of cant angle is shown. The lift-curve slope near $\alpha = 0^{\circ}$ for the model with a nose cant of 0° is also about -0.021 per degree angle of attack. At large negative angles of attack the variation of lift with cant angle is not as linear. This result might be expected because of the large incidence angle of the nose with respect to the free-stream direction. For example, for the model with 21° cant the nose is at an angle of 36° with respect to the stream at -15° angle of attack.

The use of cant causes sizable increases in lift-drag ratio. A 21° cant angle produced a lift-drag ratio of about 0.5 at an angle of attack of about -15°. It is interesting to note that the incremental increase in

the lift-drag ratio due to cant angle is essentially linear over the complete angle-of-attack and cant-angle range which was tested. This linearity did not occur for the group of models which produced lift by offset (fig. 7).

Above an angle of attack of 4°, increasing the cant angle increased the drag coefficient of the configuration. Below this angle of attack the reverse effect was true. At an angle of attack of 4° the drag coefficient was completely insensitive to nose cant.

Modified Newtonian theory was used to calculate the lift and drag variation with angle of attack for the model with a nose cant of 14°. The theory predicts only the forces on the face of the model. The prediction of both the lift coefficient and the drag coefficient was especially poor at large negative angles of attack. In the positive angle-of-attack range the theoretical prediction of the drag coefficient was good. In this range the face of the model was more nearly normal to the free-stream direction.

Figure 8 shows that the use of nose cant has no effect on the linearity of the pitching-moment curves. Neither does it affect appreciably the slope of these curves. The only effect of nose cant on pitching moment was to cause a positive increase in pitching moment with increasing nose-cant angle.

It was conjectured that holding the reference area of the canted configurations constant, as in figure 8(a), might obscure some important effects produced by canting the nose. Consequently the data were reduced to coefficient form by using as the reference area the area of the ellipse formed by the nose-afterbody juncture. (See fig. 8(b).) No important effects were noted in the data as a result of changing the reference area, except that the drag coefficient curves did not intersect at a single angle of attack for all variations in nose cant angle. Also, the angle-of-attack range at which the drag coefficient was most insensitive to nose cant angle was greater than 4°.

Effects of Nose Spikes

The use of a cylindrical, hemispherically tipped spike protruding from the center of the nose of a reentry body has been considered as a means of producing lift or exerting control forces during reentry. Such a spike on an actual flight vehicle might be gimbaled and provision would have to be made to either cool the spike or adjust the length of the spike by feeding more of the spike into the airstream to replace what would be ablated during reentry. These are only a few of the many practical problems which would have to be overcome before the use of such a configuration could be seriously considered. However, if the aerodynamic characteristics of a configuration of this type appeared sufficiently promising,

attempts to overcome the many formidable design problems would be justified. With this in mind, preliminary tests were made on the configuration shown in figure 1(d). In addition to conducting tests with spikes on the flat-faced model, tests were also conducted with spikes on nose shapes 1-A and 4-A. Some typical schlieren photographs of the shock structure which resulted for the tests with a 1.5-inch-long spike are shown in figure 9(a) and for the tests with a 0.75-inch spike in figure 9(b).

The schlieren photographs indicated that unsteady flow existed on the flat-faced models with the 1.5-inch spike, and some high-speed schlieren movies were taken of a number of configurations to confirm this fact and to define the configurations which produced this unsteady flow. For model 0-A and the 1.5-inch spike, the flow oscillated between the two flow patterns shown in the upper two schlieren photographs of figure 9(a). The frequency of the oscillations was about 500 cps at a tunnel stagnation pressure of 2/5 atmosphere and about 600 cps at a tunnel stagnation pressure of 3 atmospheres. The unsteady flow persisted to an angle of attack of about 8°, and at higher angles of attack (up to 15°) the high-speed movies showed that the flow was steady. No unsteady flow was detected on any models other than the flat-faced model except for model 4-A which had a small region of unsteady flow near the base of the spike at angles of attack near 0°. Some flow unsteadiness was observed with the 0.75-inch spike on the flat-faced model but it was of small amplitude and of a more intermittent nature than occurred with the 1.5-inch spike.

The aerodynamic characteristics of the configurations which were tested with the 0.75-inch spike are shown in figure 10. For comparison, the data for the corresponding nose shapes without the spike are shown by the dashed lines. The addition of the spike had very little effect on the lift for shapes 0-A and 4-A; however, it did produce a nonlinearity in the lift-curve data for shape 1-A. Similarly, the drag-coefficient data of nose shapes 0-A and 4-A were affected only slightly by the addition of the spike, whereas the drag-coefficient data for shape 1-A were considerably reduced in the low angle-of-attack range by the addition of a spike. This "bucket" in the drag curve must be associated with the fact that the spike on shape 1-A, with its separated flow near the base of the spike, alters the effective shape of the nose to produce a configuration with a greater nose fineness ratio. The spike did not have as great an effect on the drag for shape 0-A as for shape 1-A because the spike was too short to alter the shock structure very significantly for shape 0-A. This can be seen by comparing the upper two left-hand schlieren photographs of figure 9(b). For shape 1-A the spike penetrates the bow shock wave of the capsule to a greater extent and produces more of a bulge in the bow shock.

The pitching-moment data in figure 10 show that the addition of a spike can cause large nonlinearities.

Figure 11 shows the effect of spike length on the aerodynamic characteristics of configuration 0-A. There is very little effect on the lift data due to adding even the 1.5-inch-long spike, but the drag of the capsule is greatly reduced as the spike length is increased from 0.75 inch to 1.5 inches. The pitching-moment data are not symmetrical about $\alpha = 0^\circ$ for the configurations with spikes and therefore might be subject to some doubt. In this regard it should be remembered that for these configurations a violent oscillatory flow was taking place on the nose of the model up to an angle of attack of about 8°; however, the wind-tunnel balances indicated a steady reading since the frequency of the oscillations was very high. It is interesting to note that the pitching-moment increment produced by the 1.5-inch spike at positive angles of attack was in the negative direction. A pitching-moment increment due to lift would be in the positive direction. This result is not particularly surprising since it was expected that the spike would change the aerodynamic characteristics of the capsule primarily by producing interference effects on the face of the capsule.

L 932

Figure 12 shows the effects of spike deflection on the aerodynamic characteristics of model 1-A. The addition of an undeflected spike produced a nonlinearity in the lift curve such that near $\alpha = 0^\circ$ it had a positive slope instead of the linear negative slope of the capsule without a spike. Deflecting the spike shifted this point of lift-curve-slope reflection from $\alpha \approx 0^\circ$ to $\alpha \approx -5^\circ$ for a 10° spike deflection and to $\alpha \approx -10^\circ$ for a 20° spike deflection. The addition of a spike to the noses resulted in nearly a 50-percent reduction in the minimum drag, and the minimum drag occurred in approximately the same angle-of-attack range as the lift reflection. Actually the minimum drag occurred near $\alpha \approx -6^\circ$ for $\delta = 10^\circ$ and near $\alpha \approx -12^\circ$ for $\delta = 20^\circ$.

Although it appears that spike deflection causes a systematic alteration in the lift and drag curves, the effects of spike deflection on pitching moment are very unsystematic. Spike deflection can be used as a source for large control moments but the resulting pitching moments are very nonlinear both with regard to angle-of-attack variation (fig. 12) and variation in spike deflection (fig. 13). The variations of pitching moment with spike deflection shown in figure 13 are inconsistent with regard to the direction of the resulting moment as well as to the magnitude of this moment. It therefore appears that the use of a spike for producing control forces would require the solving of formidable aerodynamic problems as well as the problems associated with heating and the survival of the spike.

[redacted]

CONCLUSIONS

An investigation conducted in the Langley 9-inch supersonic tunnel at a Mach number of 2.91 on a reentry capsule with a series of nose shapes in order to evaluate their relative aerodynamic characteristics and the capacity of these different nose shapes to produce lift indicated the following conclusions:

1. Both slender-nosed and blunt-nosed shapes produced significant lift-drag ratios although greater lift-drag ratios were produced by the slender-nosed shapes. For example, the flat-faced nose shape produced a lift-drag ratio of 0.2 whereas the 16° half-angle nose shape produced a lift-drag ratio of 0.8. A nose shape with a cone half-angle of about 42° would have essentially no lift produced by any variation in angle of attack within the range of the tests.

2. Increasing nose fineness ratio or slenderness decreased longitudinal stability for the more slender shapes, both with the moment reference at a fixed point and with the moment reference held at the center of the planform area.

3. Modified Newtonian theory approximated the lift of both a blunt-nosed and a slender-nosed shape but considerably underpredicted the drag of the slender-nosed shape.

4. Both nose offset and nose cant produced significant increases in the lift-producing capabilities of the capsules. Offsetting the apex of the capsule with a 30° half-angle conical nose by the full capsule radius produced a lift-drag ratio of about 0.5 at an angle of attack of 0°. A 21° cant angle also produced the same lift-drag ratio at an angle of attack of about -15°. The incremental increase in lift-drag ratio due to cant angle was essentially linear for the angle-of-attack and cant-angle range of the tests.

5. Although the drag of the 50° half-angle nose shape with the nose offset increased with increasing nose offset at angles of attack above -6°, the lift-drag ratio also increased with increasing nose offset.

6. At angles of attack greater than 4° increasing the cant angle increased the drag coefficient, and at angles of attack less than 4° increasing the cant angle decreased the drag coefficient. At an angle of attack of 4° the drag coefficient was completely insensitive to any variation in cant angle.

7. Neither nose offset nor cant angle had any significant effect on the slope or linearity of the pitching-moment variation with angle of attack.

CONFI[redacted]

DECLASSIFIED

8. Slender spikes protruding from the nose of the capsules were able to produce significant lift and moments, but in some cases high-frequency oscillatory flow was encountered. Also, the pitching-moment variations were very nonlinear both with regard to angle of attack and to spike deflection.

Langley Research Center,
National Aeronautics and Space Administration,
Langley Field, Va., September 15, 1960.

REFERENCES

1. Eggers, Alfred J., Jr., and Wong, Thomas J.: Reentry and Recovery of Near-Earth Satellites, With Particular Attention to a Manned Vehicle. NASA MEMO 10-2-58A, 1958.

2. Rainey, Robert W.: Investigation of the Effects of Bomb-Bay Configuration Upon the Aerodynamic Characteristics of a Body With Circular Cross Section at Supersonic Speeds. NACA RM L55E27, 1955.

3. Burbank, Paige B., and Stallings, Robert L., Jr.: Heat-Transfer and Pressure Measurements on a Flat-Face Cylinder at a Mach Number Range of 2.49 to 4.44. NASA TM X-19, 1959.

4. Staff of the Computing Section, Center of Analysis (Under Direction of Zdeněk Kopal): Tables of Supersonic Flow Around Yawing Cones. Tech. Rep. No. 3 (NOrd Contract No. 9169), M.I.T., 1947.

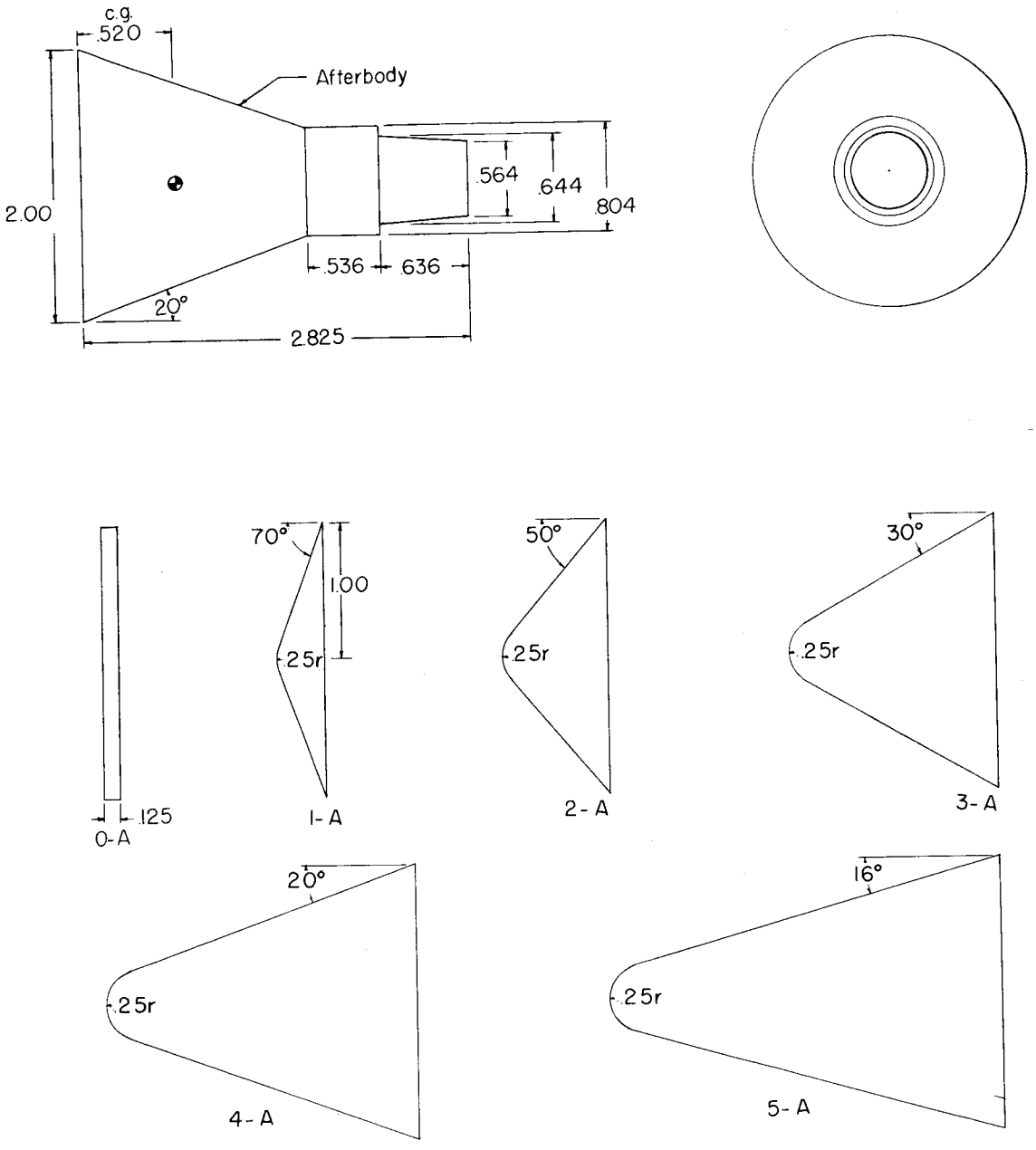

(a) Fineness-ratio series.

Figure 1.- Sketches of models and model components. All dimensions are in inches.

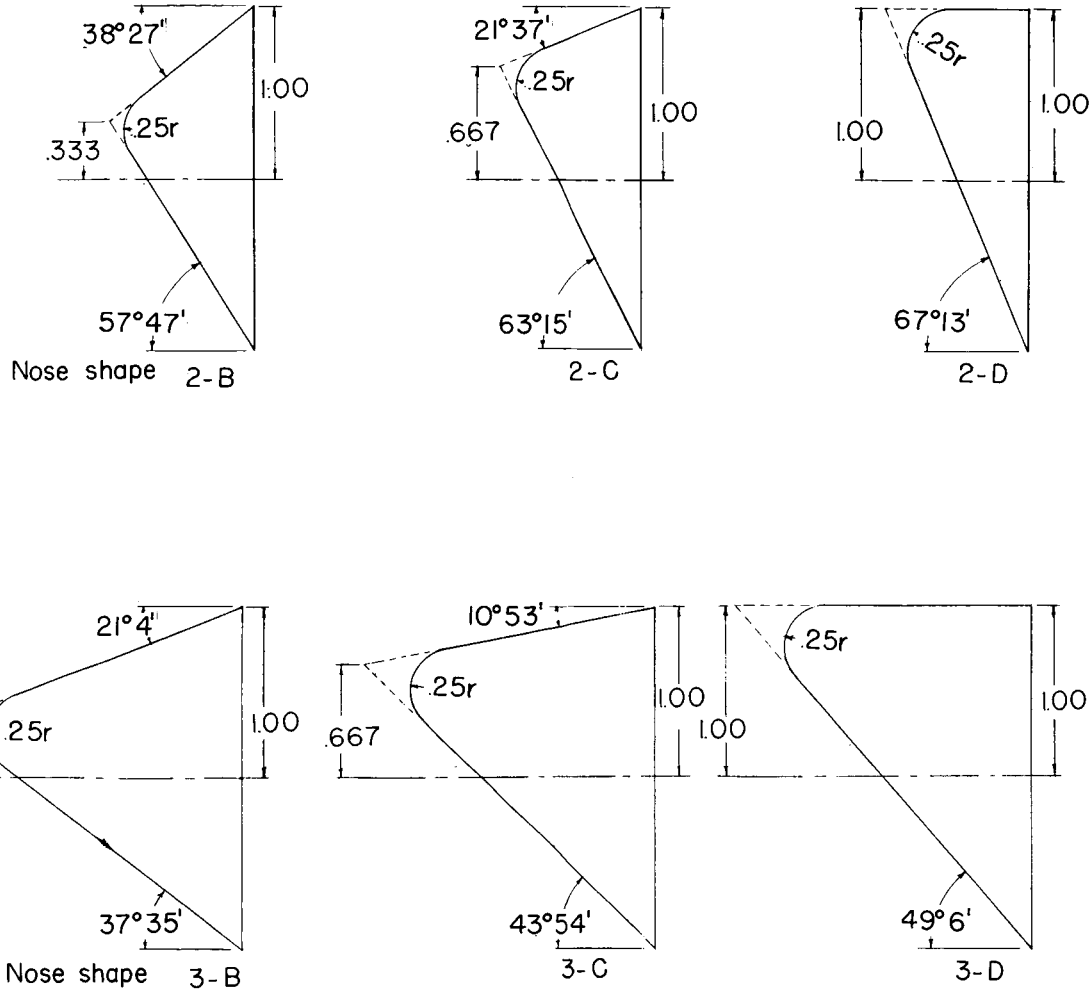

(b) Nose camber series.

Figure 1.- Continued.

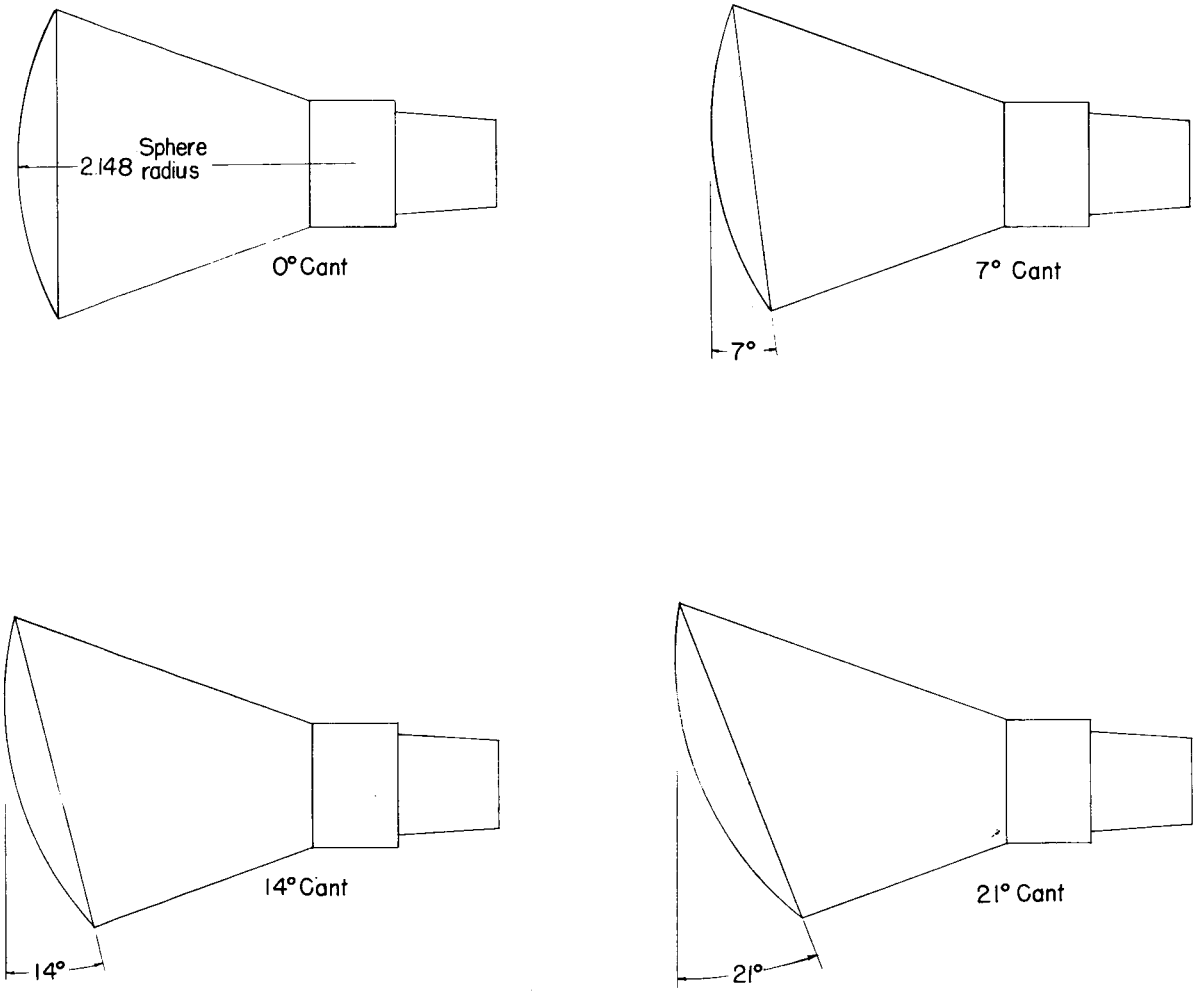

(c) Nose cant series. See back dimensions in figure 1(a).

Figure 1.- Continued.

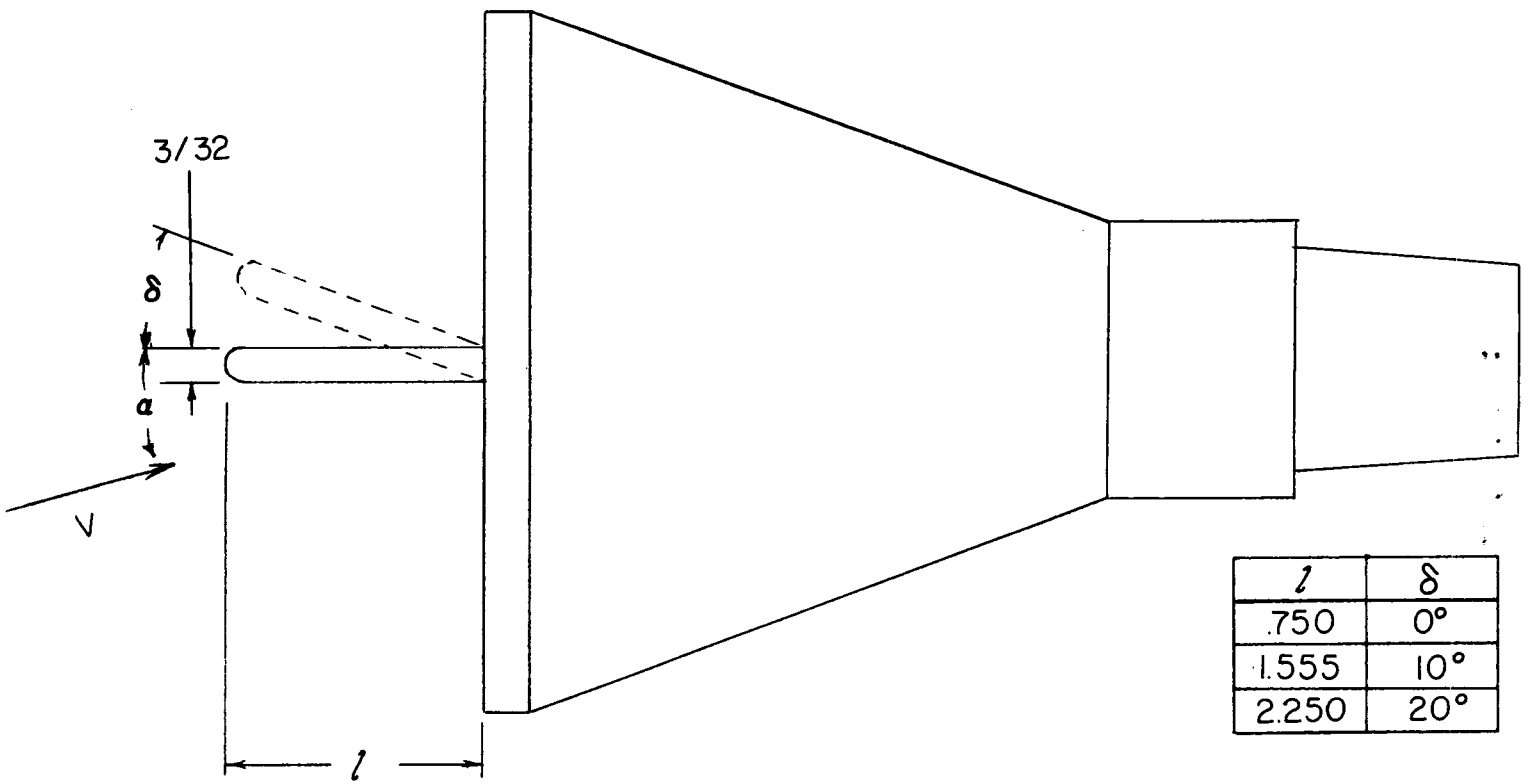

l	δ
.750	0°
1.555	10°
2.250	20°

(d) Spike with flat-faced nose shape. Spikes were also tested with models 1-A and 4-A.

Figure 1.- Concluded.

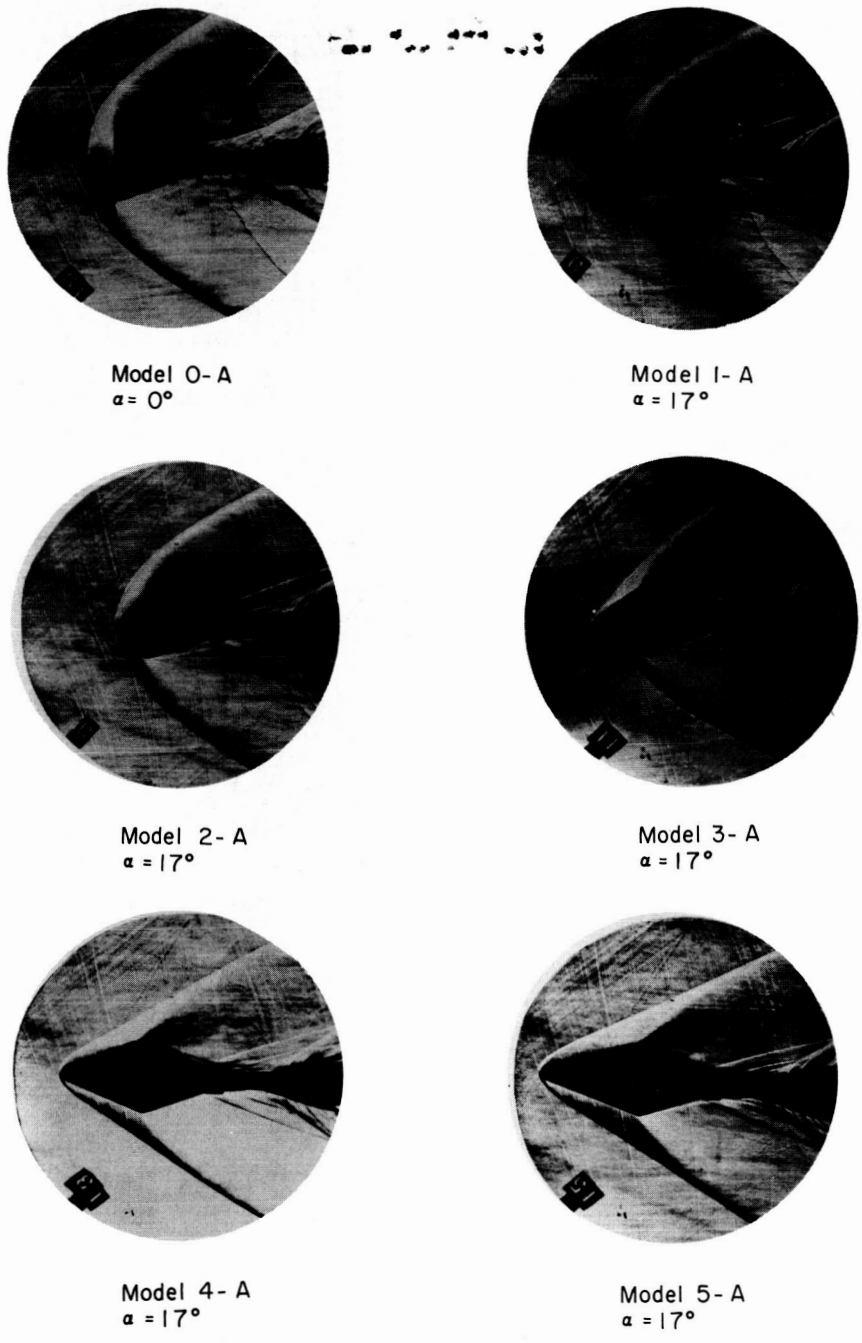

L-932

L-60-5573

Figure 2.- Some typical schlieren photographs of flow about models of various fineness ratio. Schlieren light beam in angle-of-attack plane.

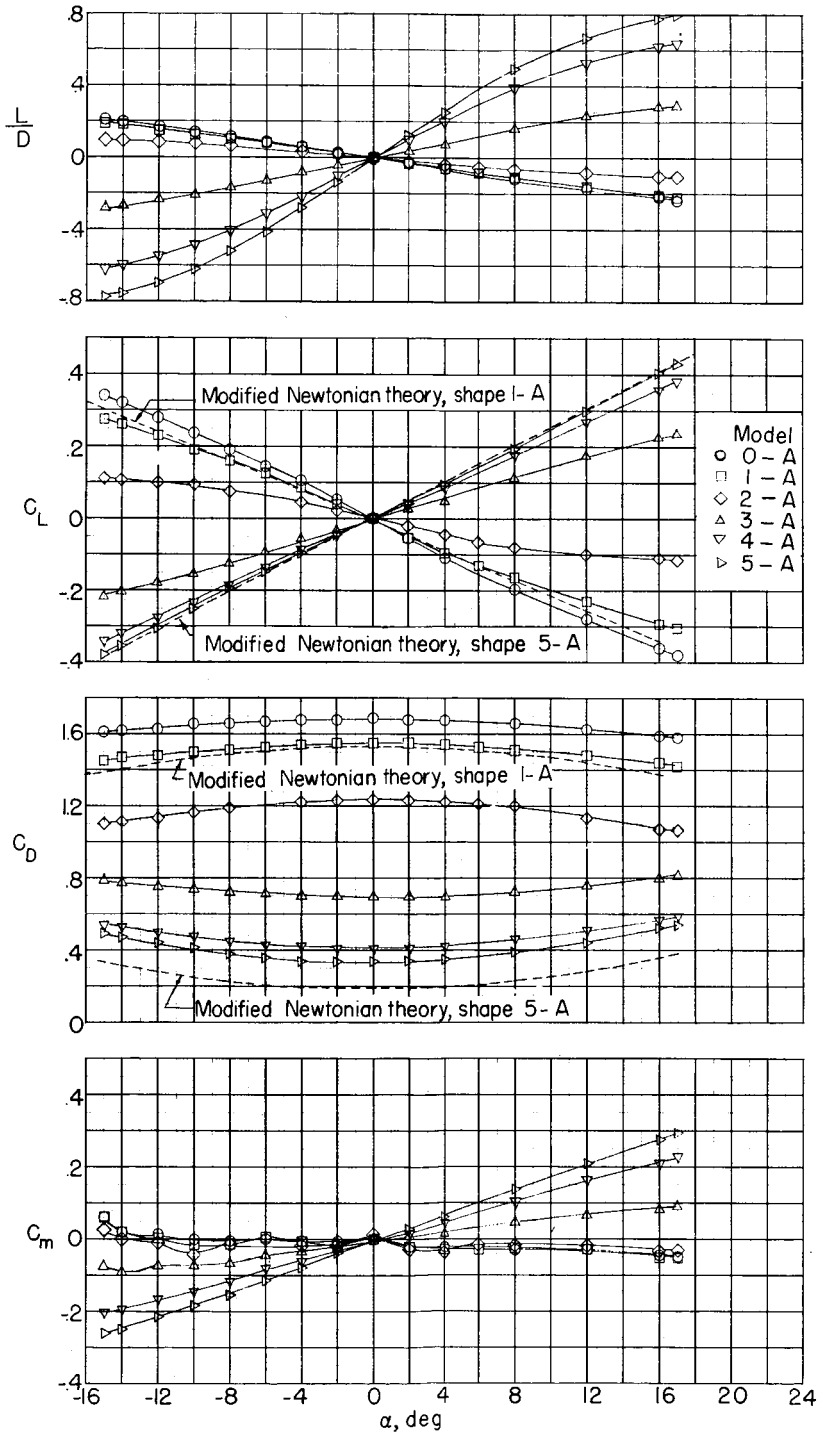

Figure 3.- Effects of nose fineness ratio on aerodynamic characteristics.

[redacted]

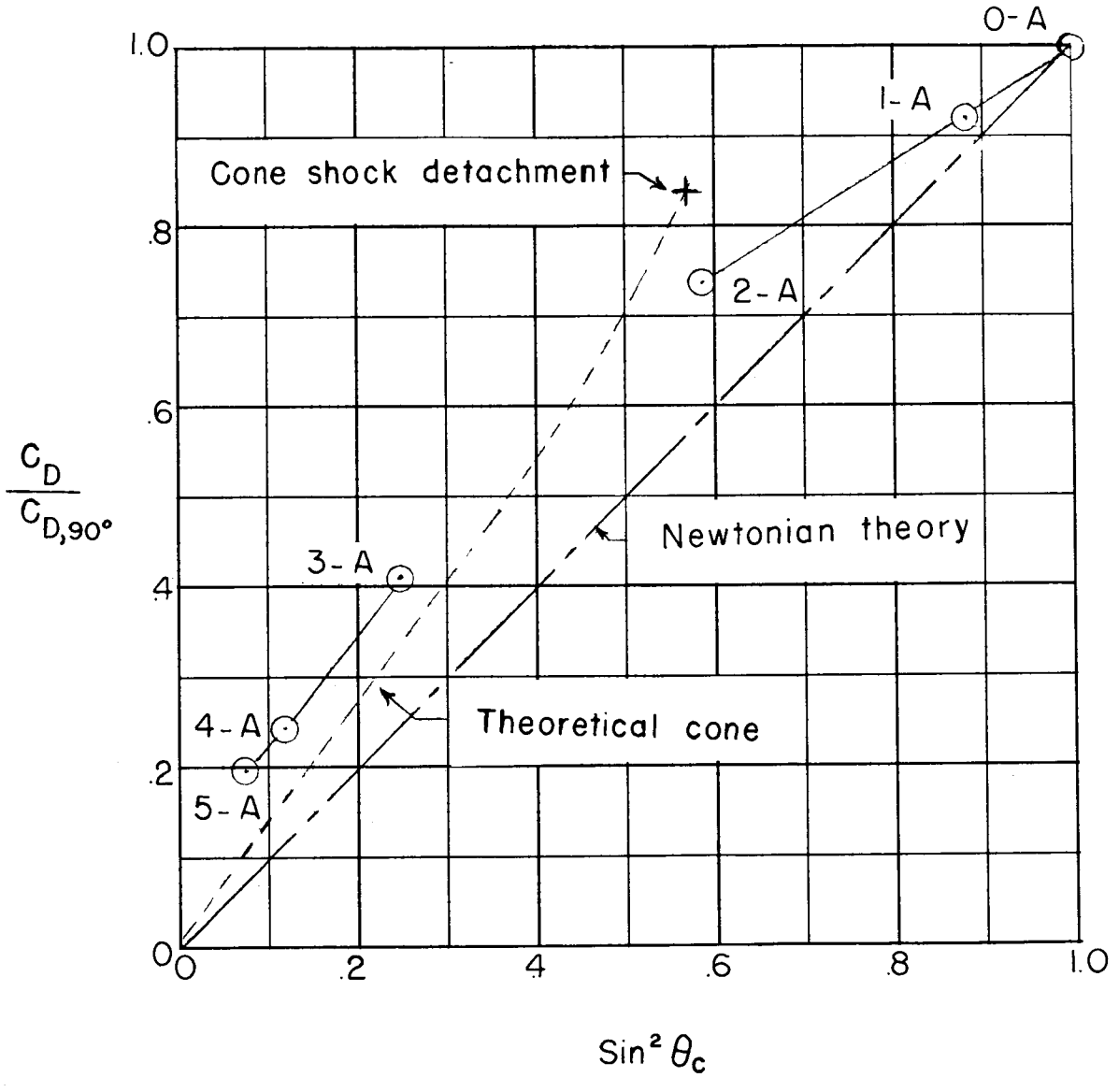

Figure 4.- Effect of nose fineness ratio on the minimum drag coefficient.

[redacted]

L-932

DECLASSIFIED

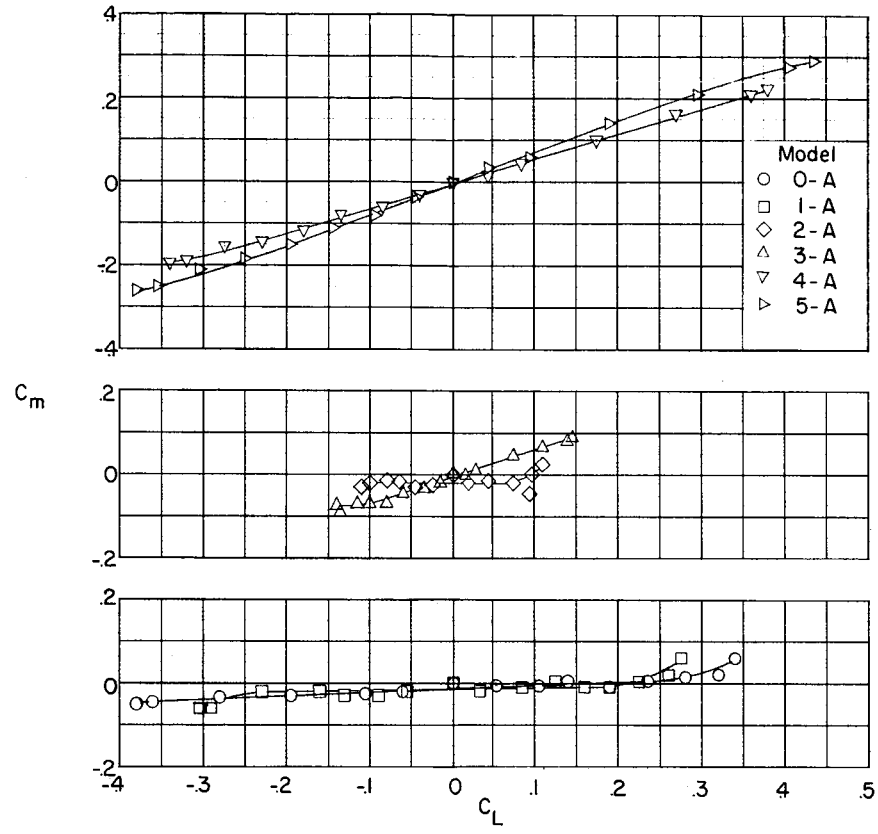

(a) Variation of C_m with C_L, showing effect of nose fineness ratio.

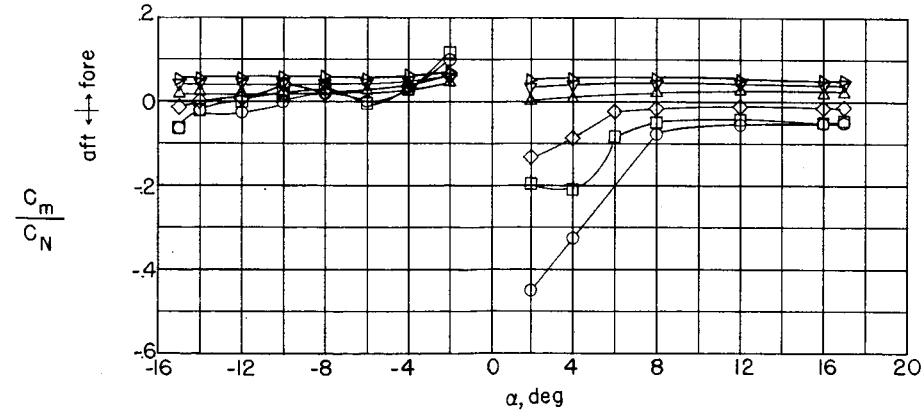

(b) Variation of center of pressure with angle of attack.

Figure 5.- Variations of stability parameters for models with moment reference at 0.52 behind nose-afterbody juncture.

CONFIDENTIAL

[redacted]

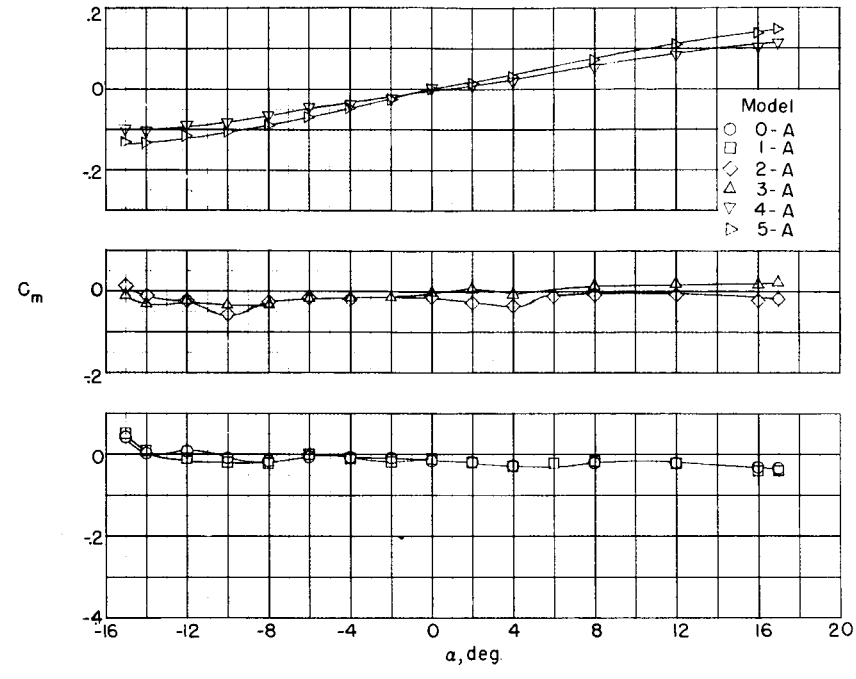

(a) Effect of fineness ratio with moment reference at center of planform area.

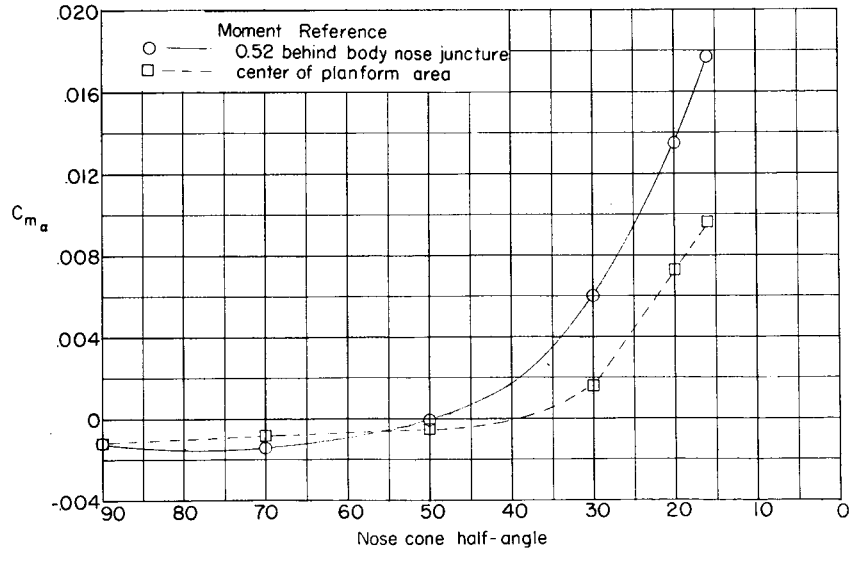

(b) Effect of nose cone angle.

Figure 6.- Variations of stability parameters.

[redacted]

L-932

DECLASSIFIED

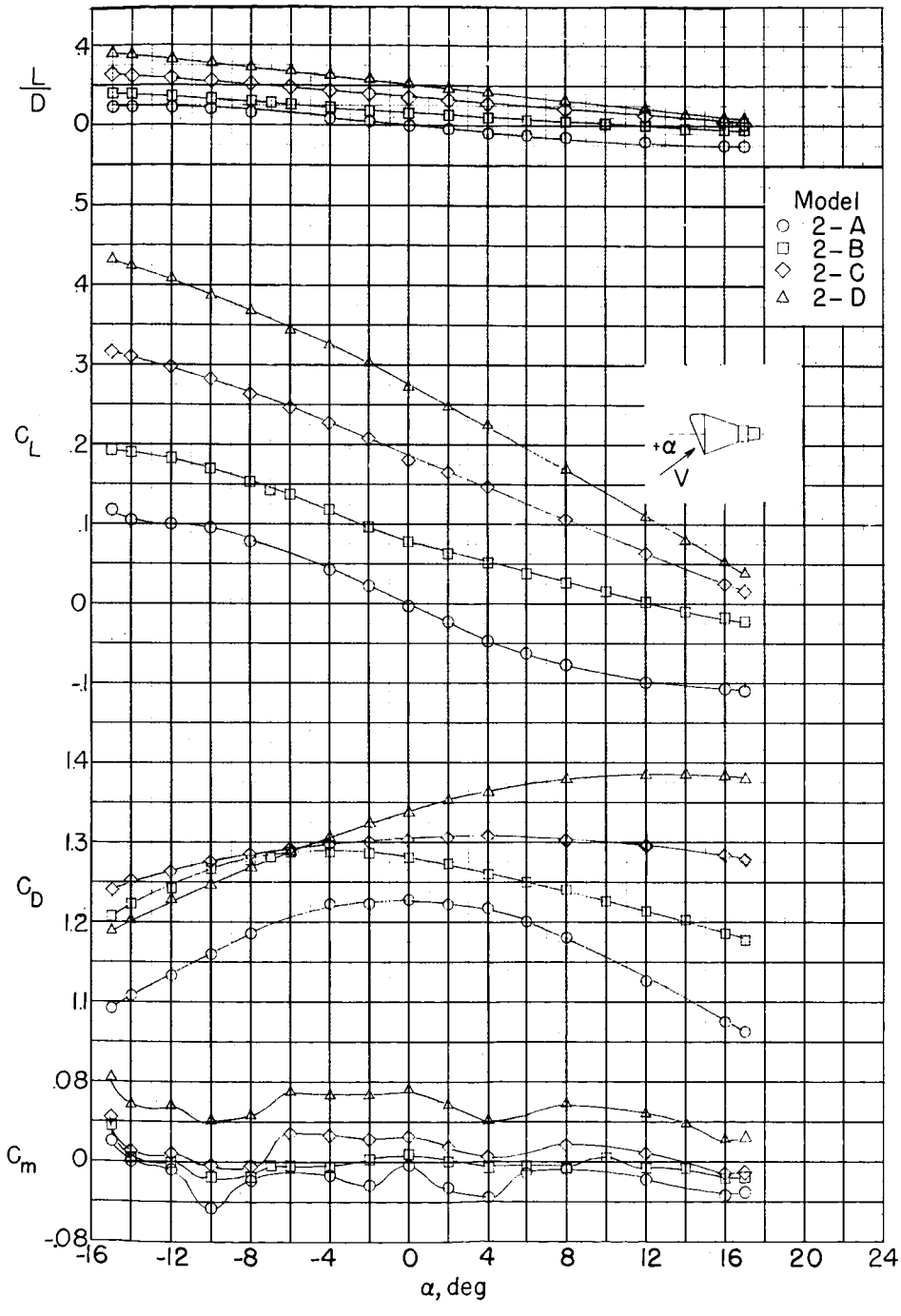

(a) Models 2-A, 2-B, 2-C, and 2-D.

Figure 7.- Effects of nose offset on aerodynamic characteristics.

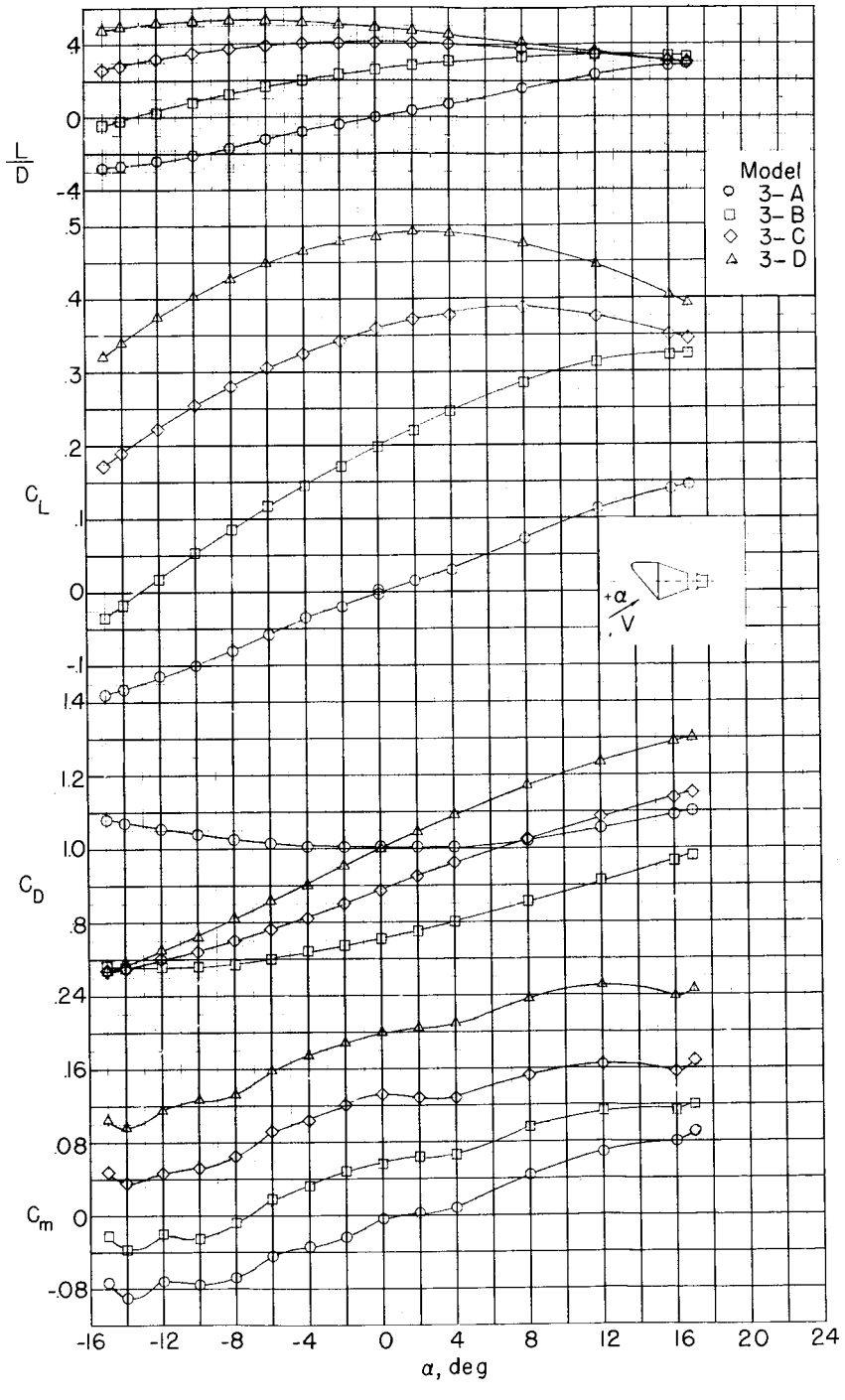

(b) Models 3-A, 3-B, 3-C, and 3-D.

Figure 7.- Concluded.

DECLASSIFIED

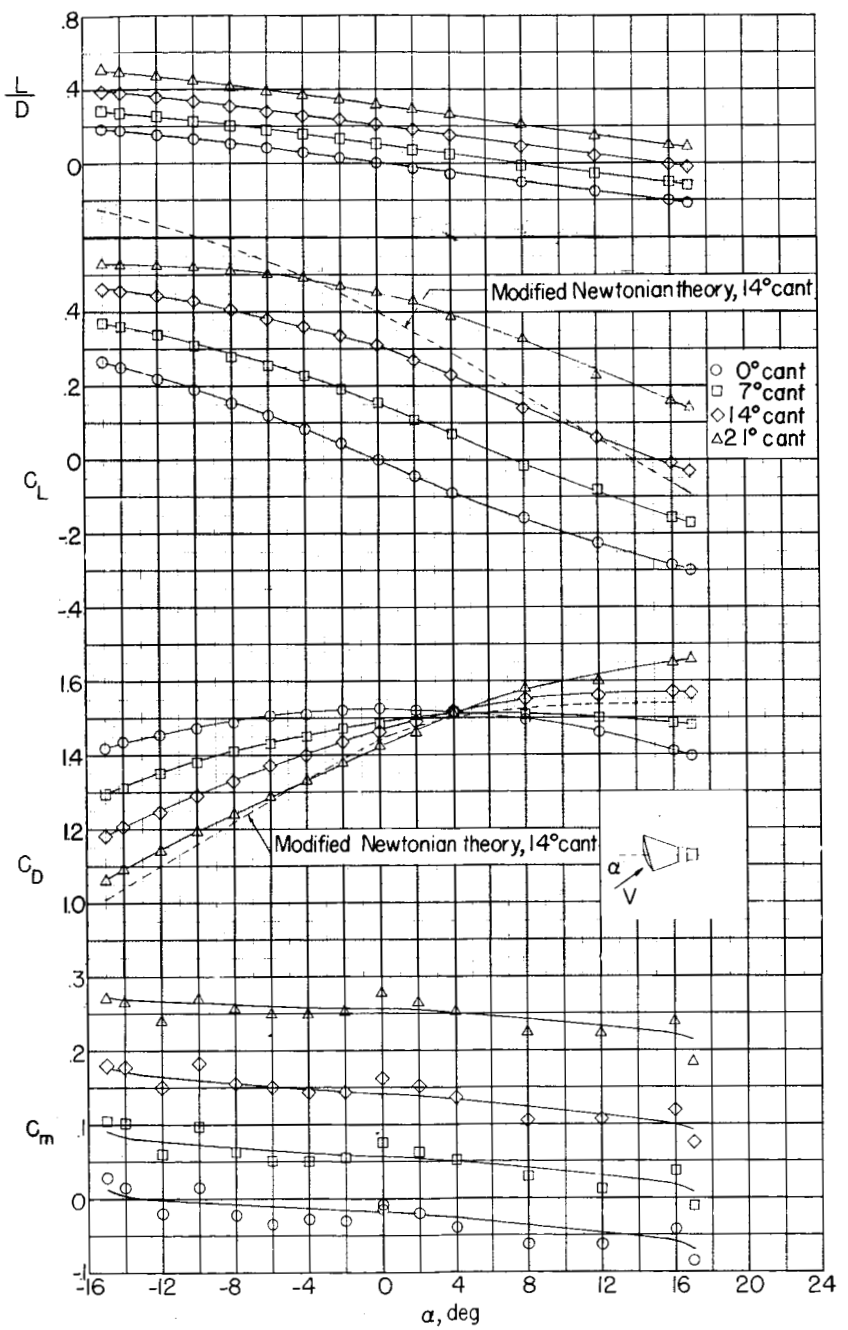

(a) Reference area is the maximum cross-sectional area of model with 0° nose cant.

Figure 8.- Effects of nose cant on aerodynamic characteristics.

C[redacted]

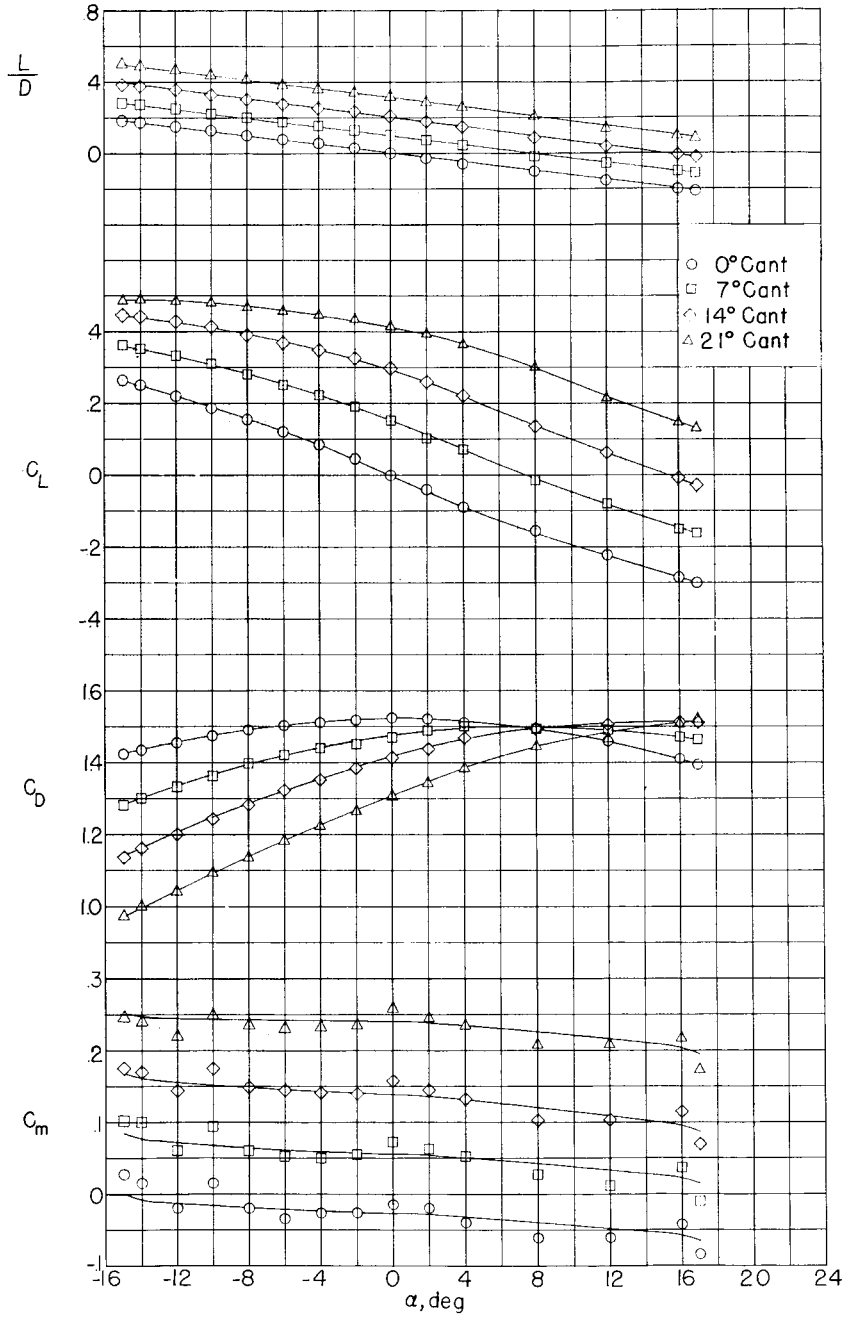

(b) Reference area is the area of the ellipse formed by the nose-afterbody juncture of each model.

Figure 8.- Concluded.

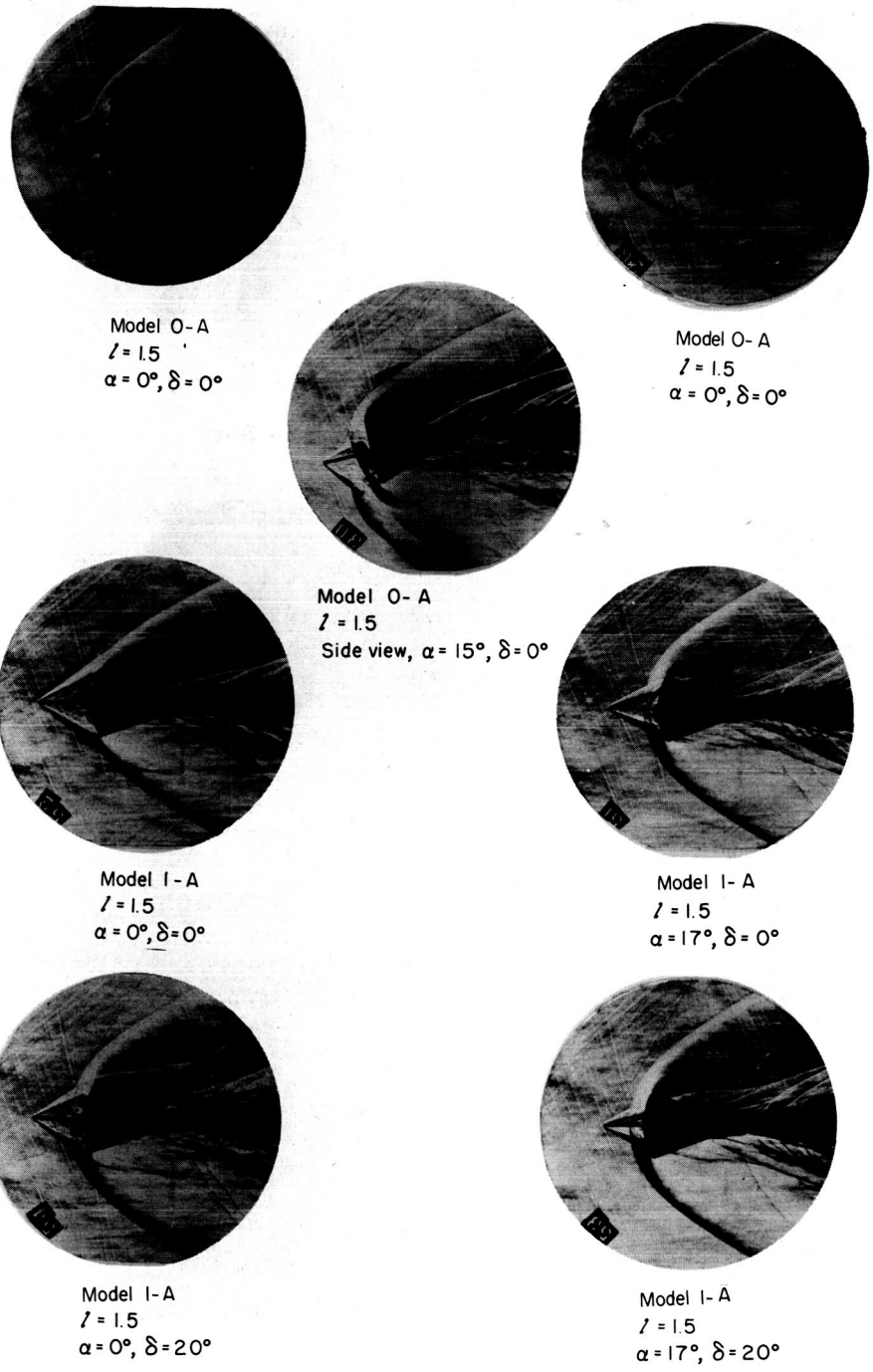

(a) Models with 1.5-inch spike. L-60-5574

Figure 9.- Schlieren photographs of shock structures. Schlieren light beam in angle-of-attack plane, except for side view.

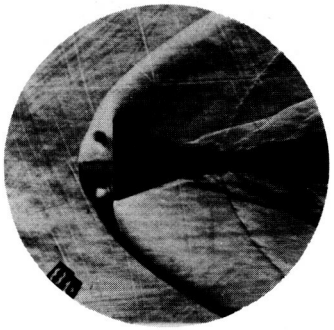

Model 0 - A
$\ell = .75$
$\alpha = 0°, \delta = 0°$

Model 0 - A
$\ell = .75$
$\alpha = 17°, \delta = 0°$

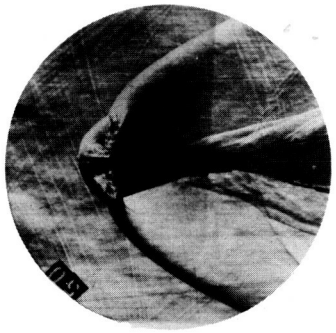

Model 1 - A
$\ell = .75$
$\alpha = 0°, \delta = 0°$

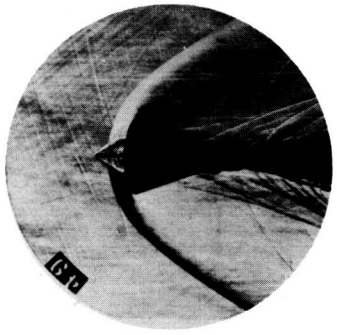

Model 1 - A
$\ell = .75$
$\alpha = 17°, \delta = 0°$

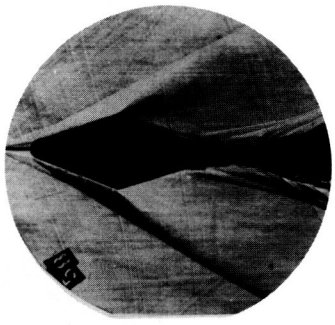

Model 4 - A
$\ell = .75$
$\alpha = 0°, \delta = 0°$

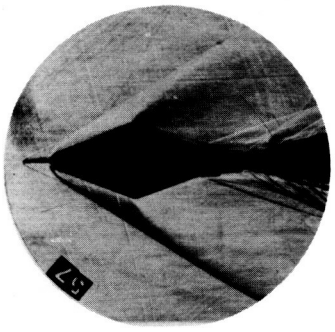

Model 4 - A
$\ell = .75$
$\alpha = 17°, \delta = 0°$

(b) Models with 0.75-inch spike. L-60-5575

Figure 9.- Concluded.

DECLASSIFIED

L-932

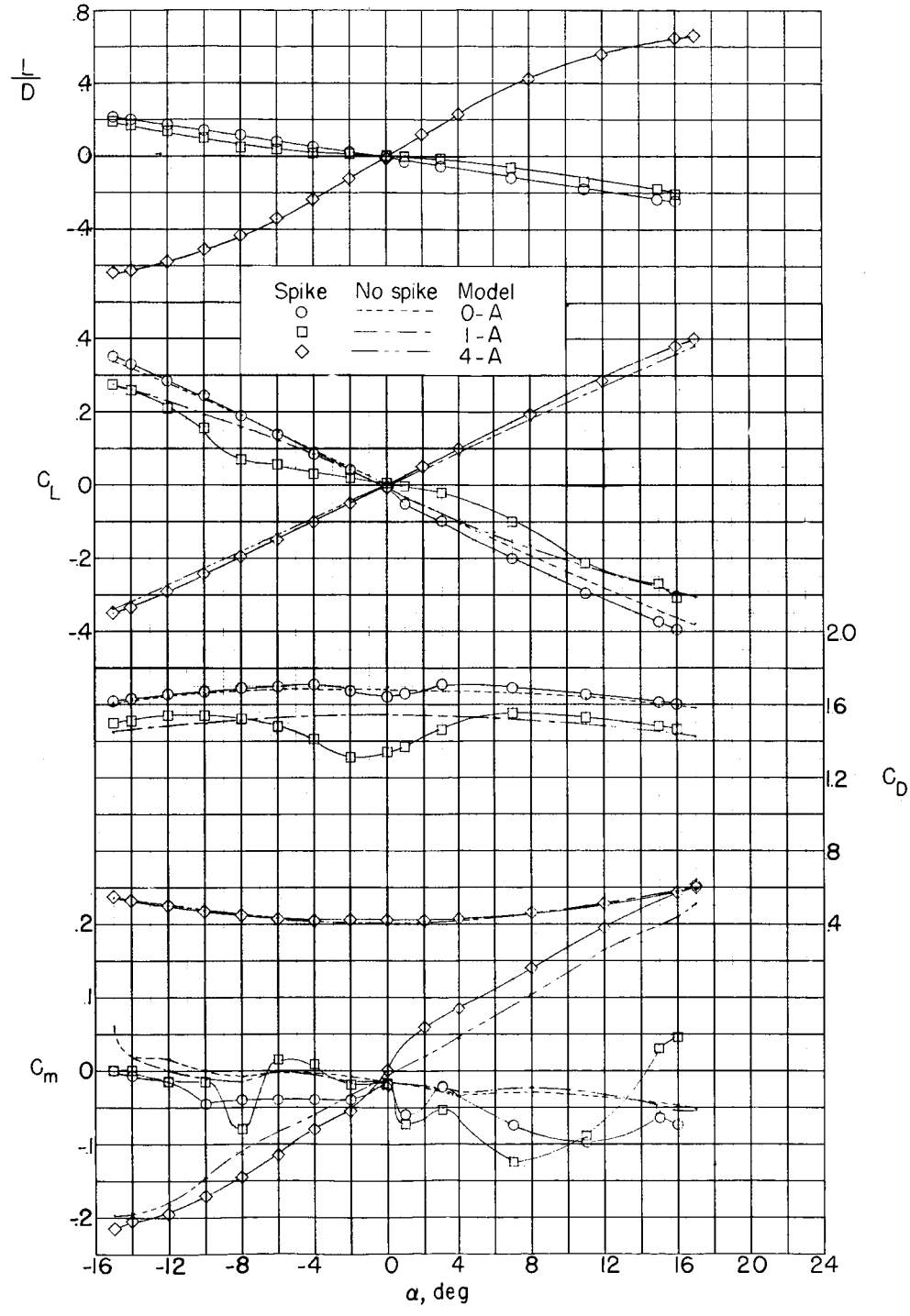

Figure 10.- Effect of 0.75-inch spike at 0° on aerodynamic characteristics of nose shapes 0-A, 1-A, and 4-A.

[redacted]

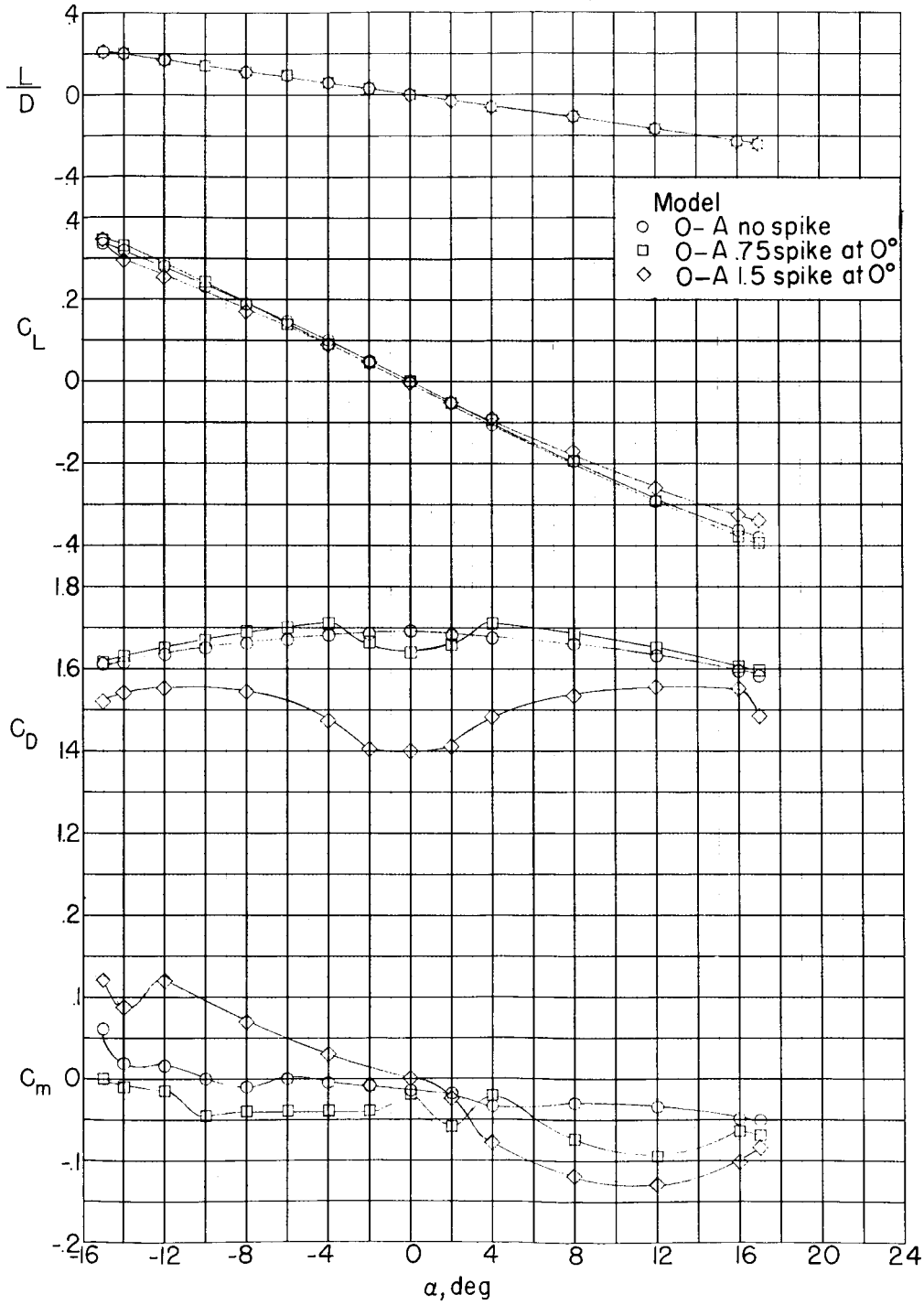

Figure 11.- Effect of spike length on aerodynamic characteristics of nose shape O-A.

[redacted]

L-932

D

DECL[redacted]FIED

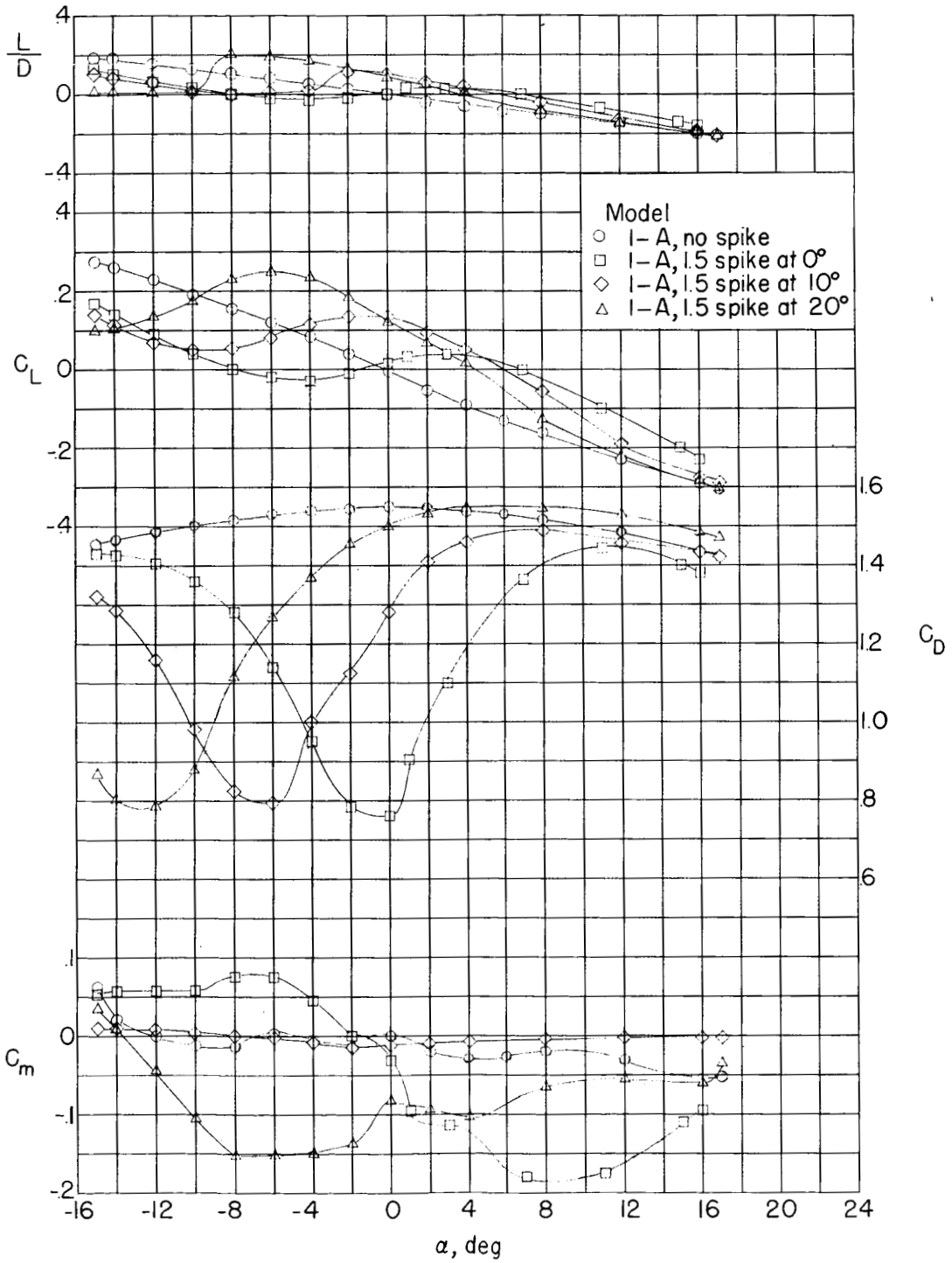

Figure 12.- Effect of spike deflection on nose shape 1-A.

[redacted]

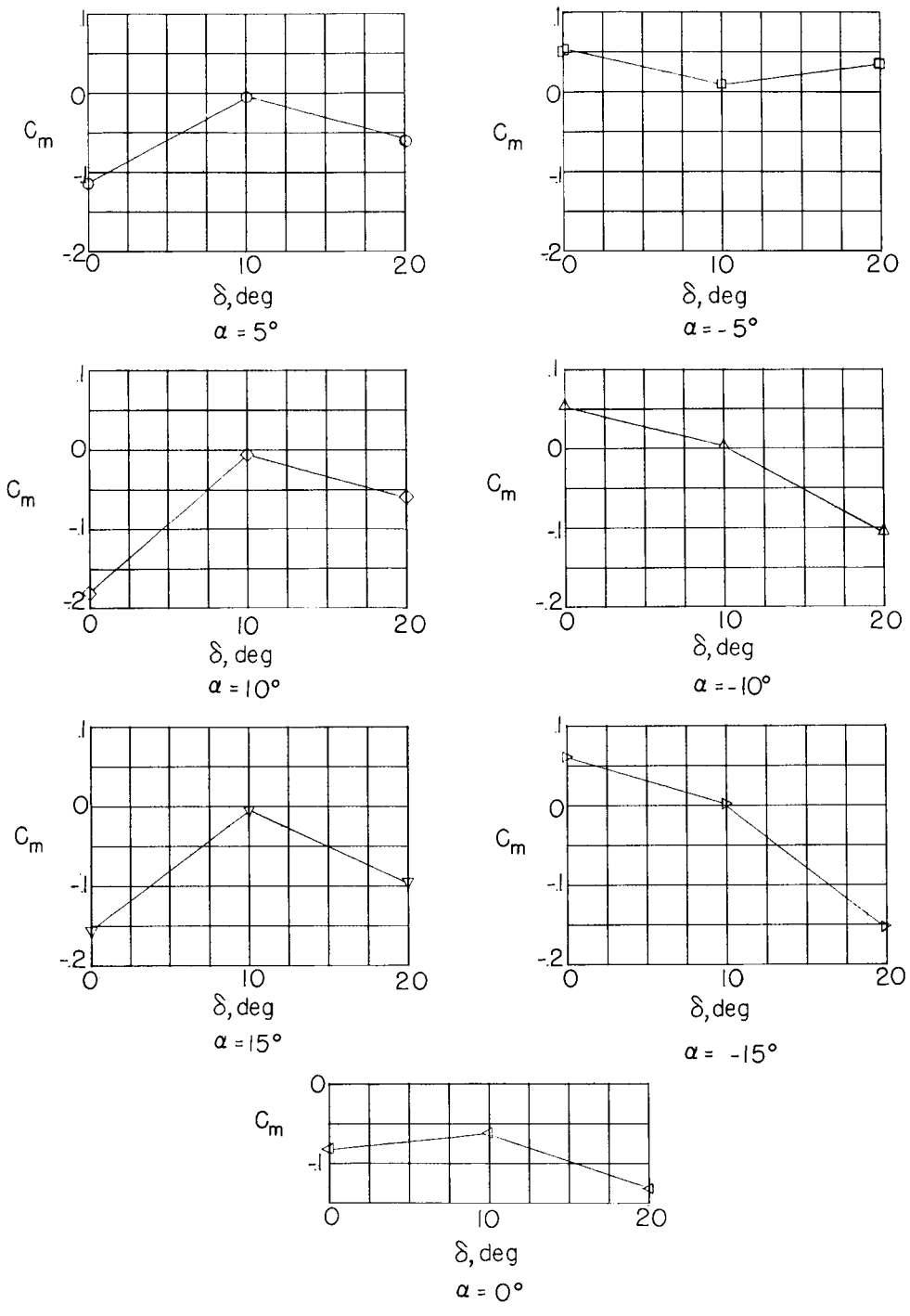

Figure 13.- Spike control effectiveness for 1.5-inch spike on nose shape 1-A.